Materials Research, Vol. 4, No. 1, 47-51, 2001.

Crystallization Kinetics of Fe-B Based Amorphous Alloys Studied *in-situ* using X-rays Diffraction and Differential Scanning Calorimetry

D.R. dos Santos[a*]***, D.S. dos Santos***[b]

[a]*Universidade Estadual do Norte Fluminense / CCT-LCFis, Campos dos Goytacazes - RJ, Brazil*
[b]*Universidade Federal do Rio de Janeiro / PEMM-COPPE, Rio de Janeiro - RJ, Brazil*

Received: November 22, 2000; Revised: January 16, 2001

The crystallization processes for the amorphous metallic alloys $Fe_{74}B_{17}Si_2Ni_4Mo_3$ and $Fe_{86}B_6Zr_7Cu_1$ (at. %) were investigated using X-rays diffraction measurements performed *in-situ* during Joule-heating, with simultaneous monitoring of the electrical resistance. We determined the main structural transitions and crystalline phases formed during heating, and correlated these results to the observed resistance variations. As the annealing current is increased, the resistance shows an initial decrease due to stress relaxation, followed by a drop to a minimum value due to massive nucleation and growth of α-Fe nanocrystals. Further annealing causes the formation of small fractions of Fe-B, B_2Zr or ZrO_2, while the resistance increases due to temperature enhancement. *In situ* XRD measurements allowed the identification of metastable phases, as the γ-Fe phase which occurs at high temperatures. The exothermal peaks observed in the differential scanning calorimetry (DSC) for each alloy corroborate the results. We also have performed DSC measurements with several heating rates, which allowed the determination of the Avrami exponent and crystallization activation energy for each alloy. The obtained activation energies (362 and 301 kJ/mol for Fe-B-Zr-Cu; 323 kJ/mol for Fe-B-Si-Ni-Mo) are comparable to reported values for amorphous iron alloys, while the Avrami exponent values (n = 1.0 or n = 1.2) are consistent with diffusion controlled crystallization processes with nucleation rates close to zero.

Keywords: *crystallization kinetics, iron alloys, X-rays, DSC*

1. Introduction

Great scientific effort has been developed in last years in order to predict and control the crystallization processes of metallic glasses, since several attractive properties of the resulting material are strongly related to the final attained microstructure. For instance, it has been shown that the nanocrystalline structure presented by Fe-Cu-Nb-Si-B alloys annealed at 813 K during 1 h is responsible for their excellent soft-magnetic properties[1,2]. A similar behavior is observed for alloys of the Fe-B-Zr-Cu family[3,4]. Several techniques have been applied to the study of crystallization processes in glassy metals, such as ferromagnetic resonance[5,6], differential scanning calorimetry[7,8], Mössbauer spectroscopy[9], small angle X-rays scattering[10,11], and electrical resistance variations[12,13]. On the other hand, there is an increasing number of studies which use synchrotron radiation sources, whose high intensity allow *in-situ* measurements to follow structural evolutions in real time.

Joule heating (JH) is a fast and highly reproducible annealing technique for amorphous metallic ribbons. It is worth noticing that it is a non-isothermal treatment, since the temperature in the sample depends on its resistivity, which, in turn, depends on the sample's microstructure, that undergoes transformations upon heating, thus changing the temperature itself. A theoretical model that relates the structural transformations to the electrical resistance variations during Joule heating at a constant applied dc current was proposed by Allia *et al.*, and used to estimate the temperature variations in an Fe-Ni-P-B alloy[14,15]. Measurements of the temperature evolution of Fe-B-Zr-Cu alloys during Joule annealing have been recently reported, showing a continuous temperature increase as the annealing current is linearly enhanced[16].

e-mail: drsantos@uenf.br
Trabalho apresentado no 14º CBECIMAT , Águas de São Pedro, Dezembro 2000

As regards the crystallization kinetics during isothermal treatments, the time evolution of the crystalline volume fraction, f_v, is given by the Johnson-Mehl-Avrami equation:

$$f_v = 1 - \exp(-Kt^n) \quad (1)$$

where K and n are time-independent parameters. A simple manipulation of Eq. (1) shows that, K and n can be determined by plotting the measured data, f_v, as:

$$\ln[-\ln(1-f_v)] = \ln K + n \ln t \quad (2)$$

In the case of continuous heating, it can be shown that for $E >> RT$ the following relations are true[7,17,18]:

$$\beta \frac{E}{K_p R T_p^2} = 1 \quad (3)$$

$$\left(\frac{dx}{dt}\right) = 0{,}37\, nK_p \quad (4)$$

$$\frac{d\left[\ln\left(\frac{T_p^2}{\beta}\right)\right]}{d\left[\frac{1}{T_p}\right]} = \frac{E}{R} \quad (5)$$

where β is the heating rate, E is the activation energy, R is the gas constant, n is the Avrami exponent and the index p refers to the variables at a crystallization peak, *i.e.*, T_p is the temperature of a peak, K_p is the rate constant at the peak and $(dx/dt)_p$ is the crystallization rate at the peak. If T_p^2/β is measured in a series of exothermals taken at different heating rates, the plot of $\ln(T_p^2/\beta)$ as a function of $1/T_p$ should be a linear function with slope E/R. The set of equations given by Eqs. 3 and 4 can then be used to determine the Avrami exponent n as an average of the set of parameters obtained for different heating rates.

In the present work, we investigate the crystallization process of two Fe-based amorphous metallic alloys, using X-rays diffraction (XRD) measured *in-situ* during Joule annealing, and simultaneously monitoring the electrical resistance variations. DSC measurements with different heating rates were also performed in order to determine important crystallization parameters, such as the activation energy and the Avrami exponent.

2. Experimental Procedures

The amorphous alloys of nominal composition $Fe_{74}B_{17}Si_2Ni_4Mo_3$ and $Fe_{86}B_6Zr_7Cu_1$ (at. %) were rapidly quenched from the melt by planar flow on a fast rotating cylinder, producing high quality metallic ribbons of thickness 25 ± 1 μm. Samples cut from each amorphous alloy were submitted to JH with an effective length of 10 mm between electrical contacts. The sample was firmly clamped at both ends by two pairs of electrical contacts, using a sample holder specially designed to minimize conduction thermal losses and keep the ribbon perpendicular to the X-ray beam, allowing for sample expansion during heating. The applied dc current was varied from 0 to 3.0 A while the voltage drop across the sample was measured via two independent contacts. The heating procedure was computer controlled, thus allowing the on-line analysis of the *R(I)* curve. During annealing, the sample was kept in vacuum (10^{-2} mbar) to avoid oxidation and minimize convective thermal losses.

It was shown in a previous work that for a constant applied current the structural changes occur during the initial 10 s (see Fig. 1 in Ref. 12). Consequently, in the case of a step by step enhancement of the annealing current each increment ΔI should be applied after a minimum waiting time Δt_{min} = 10 s. For longer time intervals one obtains reproducible *R(I)* curves, suggesting that the crystallization process is also reproduced. Using the characteristic *R(I)* curve as a guide, different current values were selected for *in situ* measurements of X-ray diffraction intensities. For each thermal treatment we performed 12 sequential exposures, where XRD patterns were registered on a curved Imaging Plate in the angular range $10° \le 2\theta \le 152°$. The experimental setup for *in situ* XRD measurements requires detector displacement between film expositions, so we selected long time intervals Δt = 450 s for each current increment ΔI = 0.1 A. After waiting 20 s for temperature stabilization in the sample, the remaining 430 s were used for recording XRD spectra. These measurements were carried out at the SAXS beam-line of the LNLS – National Synchrotron Light Laboratory, Brazil[19,20]. The wavelength λ = 1.7574 Å was selected in order to minimize the attenuation factor and fluorescence from Fe atoms in the samples, and the beam dimensions over the sample were 0.8 x 3.0 mm. Diffraction curves from a standard Al_2O_3 powder with controlled grain size (1 μm) were measured at room temperature in the same experimental geometry for 2θ calibration. The average grain size was calculated from the full width at half maximum of the 110 α-Fe reflection, using the Scherrer formula (for details see Ref. 12).

DSC measurements were performed on a Shimadzu D-50 calorimeter from room temperature to 1000 K, using heating rates of 2, 5, 10, 20 and 30 K/min. Some treatments were interrupted at particular temperatures, and XRD patterns were obtained at room temperature using a Siemens D5000 diffractometer, in order to evaluate the corresponding stage of crystallization. There is a great similarity between JH and DSC heating procedures, since both are non-isothermal treatments. As the applied current is increased the sample temperature continuously increases[16]. On the other hand, the connection between the applied JH heating rate $\Delta I / \Delta t$ and the resulting temperature rate $\Delta T / \Delta t$ should be experimentally determined, since it depends on the balance between the heating power (I^2R) and

the thermal losses. In Ref. 16, for example, it was shown that a Joule heating rate of 0.003 A/s produced an average temperature rate of 50 K/min for Fe-B-Zr-Cu ribbons.

3. Results and Discussion

Figure 1 presents XRD spectra obtained at different annealing currents. Figure 2 shows the corresponding *R(I)* curves, where solid dots represent the points selected for exposure to X-rays. The electrical resistance *R* showed a typical behavior as a function of the applied current, and very similar *R(I)* curves were obtained for both alloys. For the Fe-B-Zr-Cu alloy, the typical *R(I)* curve initially decreases, then presents a slow increase up to about 1.1 A. In this range the sample is still amorphous, thus the initial resistance decrease is interpreted as internal stress relaxation in the as-quenched material, followed by a resistance increase due to a temperature enhancement. Further annealing causes a resistance drop to a minimum at 1.7 A, while XRD spectra show the nucleation and growth of α-Fe nanocrystals, with grain sizes of about 10 nm, and increasing crystalline volume fraction in this current range. During the massive Fe crystallization the resistance is reduced down to a minimum, and then the samples presents a new metallic behavior with a rapid temperature increase due to a larger thermal coefficient of resistance (TCR)[13,16]. A similar behavior was observed for the Fe-B-Si-Ni-Mo alloy, with the beginning of structural ordering shifted to a higher current value (1.4 A), and the formation of larger α-Fe grains, about 40 nm in size.

In the case of Fe-B-Si-Ni-Mo samples, evolution of α-Fe phase occurs simultaneously with the formation of metastable Fe_2B, which for more severe heating conditions transforms into a stable Fe_3B phase. On the other hand, in the case of Fe-B-Zr-Cu samples small fractions of ZrO_2 (at 1.6 A) and B_2Zr (at 2.0 A) were observed, which do not show a significant intensity evolution from 2.0 to 3.0 A. In addition an allotropic transition from α-Fe (bcc) to a γ-Fe (fcc) phase was observed at a high value of applied current (2.4 A). This process was found to be of a transient nature for 450 s step conditions, probably due to thermal losses since for a faster heating rate (Δt = 150 s) it was found to be permanent up to applied currents of 3.0 A. For all the identified phases, the diffraction profiles were simulated and fitted to the experimental data, yielding lattice parameters about 1.1 % larger than the room temperature values.

Figure 3 shows DSC curves for both Fe-B-Zr-Cu and Fe-B-Si-Ni-Mo amorphous metallic alloys, obtained at a heating rate of 30 K/min. Samples of the Fe-B-Zr-Cu alloy present two distinct exothermal peaks, and this behavior is independent of the applied heating rate (2, 5, 10, 20 or 30 K/min). On the other hand, the crystallization of Fe-B-Si-Ni-Mo samples followed different kinetics according to the applied heating rate, as described below.

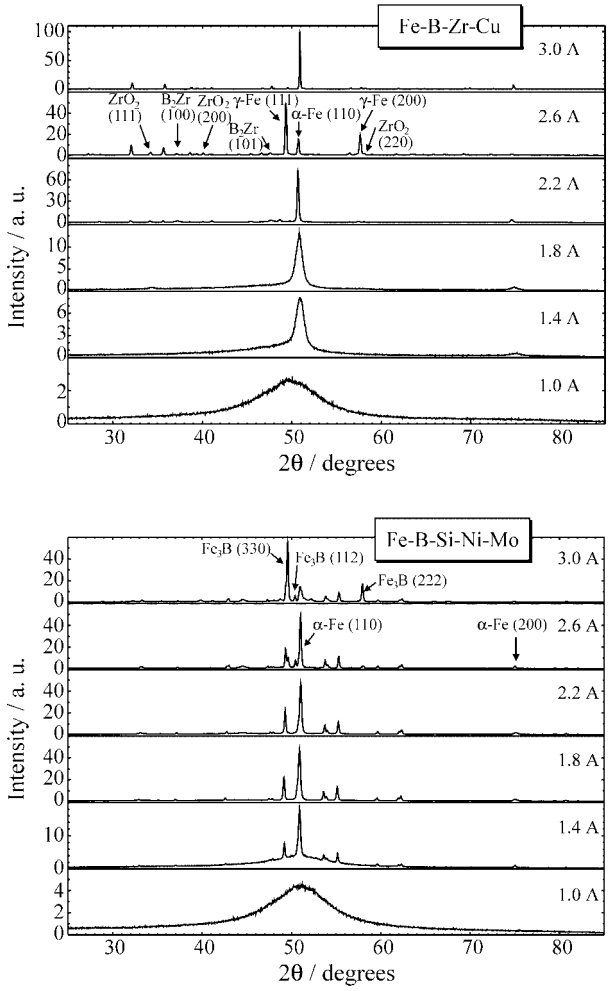

Figure 1. Evolution of the X-ray diffraction intensities measured *in-situ* during Joule heating. At 1.0 A the samples are still amorphous. The crystalline phases are indicated, with the corresponding peak indexes.

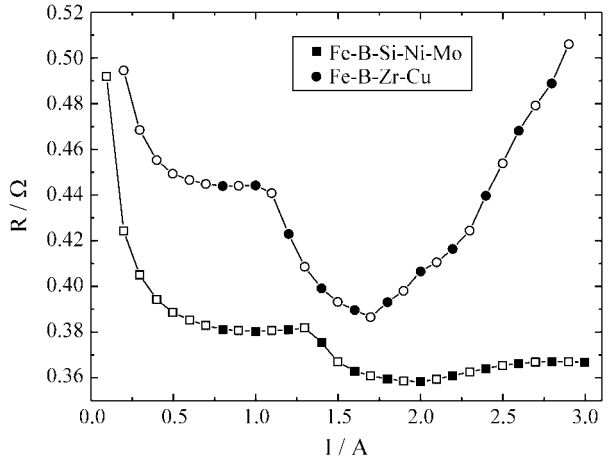

Figure 2. Electrical resistance variations measured on-line during Joule heating. Solid dots correspond to the annealing currents selected for XRD measurements.

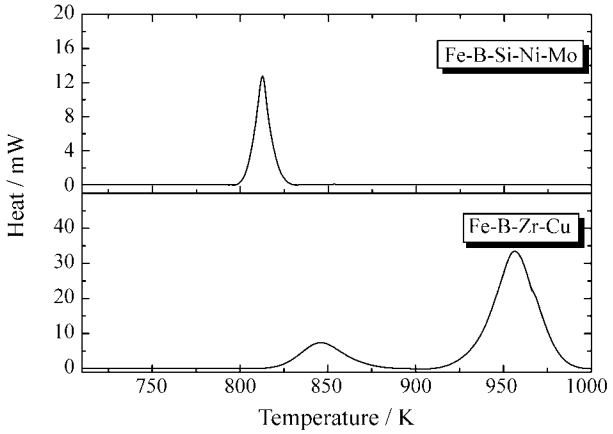

Figure 3. Differential scanning calorimetry curves obtained at a heating rate of 30 K/min

DSC curves for annealing at 2 K/min showed three peaks, the first one being the most intense, suggesting a crystallization process with three well resolved exothermal reactions. For annealing at 5 K/min, however, only two exothermal peaks were detected, the first one being again the most intense. For faster annealing conditions (heating rate equal or superior to 10 K/min) DSC curves presented only one peak, suggesting that all the structural transitions occur simultaneously at about the same temperature. Equations 3 to 5 were applied to our DSC scans in order to determine the crystallization activation energy *E* and the Avrami exponent *n*, which depends on the predominant crystallization mechanism. Figure 4 shows the plots obtained for $ln\,(T_p^2/\beta)$ *vs.* $1/T_p$ and the linear functions used in the determination of the activation energies for both alloys. For the Fe-B-Zr-Cu alloy it was possible to evaluate the crystallization parameters for each independent exothermal reaction, and the results are presented in Tables 1 and 2.

The obtained values of the Avrami exponent were $n = 1.0$ for Fe-B-Si-Ni-Mo and for the first reaction in Fe-B-Zr-Cu alloy, while the second reaction presented a slightly larger value, $n = 1.2$. These results are consistent with a diffusion controlled crystallization process, with nucleation rate near zero[21]. The obtained activation energies are comparable to previously reported values for several amorphous metallic alloys submitted to isothermal

Table 2. Crystallization parameters of $Fe_{74}B_{17}Si_2Ni_4Mo_3$ measured by DSC.

β (K/min)	*N*	$\langle n_1 \rangle$	E_1 (kJ/mol)
2	0.98		
5	1.00		
10	1.01	1.0	323 ± 16
20	1.06		
30	1.07		

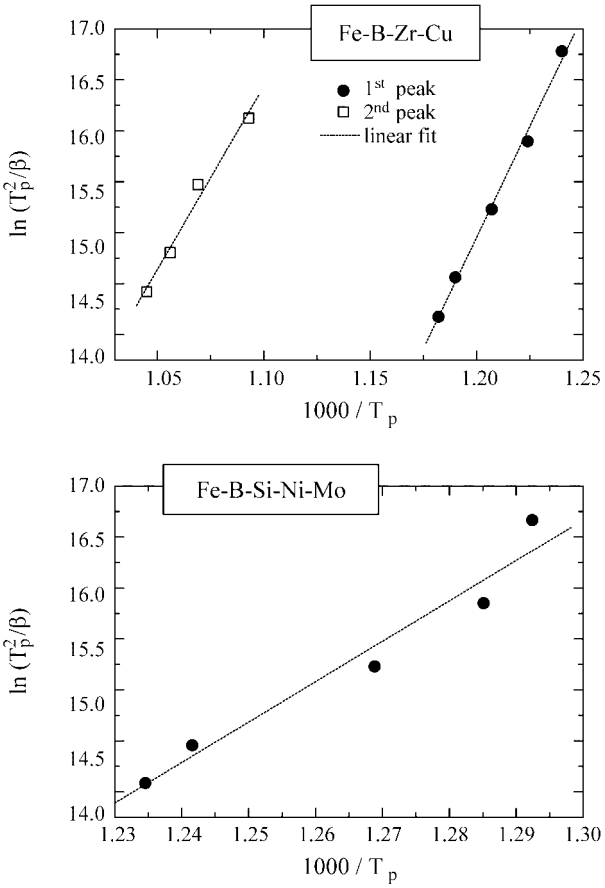

Figure 4. Plots for determination of the activation energy *E* from a set of DSC scans with different heating rates (2, 5, 10, 20 and 30 K/min). In the case of the Fe-B-Zr-Cu alloy, this analysis was performed for each observed exothermal reaction.

Table 1. Crystallization parameters of $Fe_{86}B_6Zr_7Cu_1$ measured by DSC.

β (K/min)	n_1	n_2	$\langle n_1 \rangle$	$\langle n_2 \rangle$	E_1 (kJ/mol)	E_2 (kJ/mol)
2	0.89	-				
5	0.93	1.18				
10	0.97	1.19	1.0	1.2	362 ± 14	301 ± 20
20	0.99	1.20				
30	1.02	1.34				

annealing.[5,6,8] This result shows that, though DSC technique demands a continuous heating of the sample, it is a suitable technique for studies on the crystallization kinetics of these materials.

4. Conclusions

DSC and X-ray diffraction measurements during Joule heating have proved to be powerful techniques to analyze in real time the disorder-order transition for amorphous metallic ribbons. Both Fe-B based alloys presented an evolution of the crystallization products at different stages of annealing. For the Fe-B-Zr-Cu alloy it was observed the formation of α-Fe nanocrystals with increasing crystalline volume fraction up to 1.8 A, followed by the formation of small fractions of ZrO_2 and B_2Zr which do not show a significant intensity evolution as the current increases. At high values of applied currents, that correspond to higher temperatures, it was observed a phase transition from α-Fe (bcc) to a unstable γ-Fe phase (fcc), which reverts to bcc at 3.0 A. For the Fe-B-Si-Ni-Mo alloy, the crystallization and growth of larger α-Fe nanocrystals occur simultaneously with the formation of metastable Fe_2B, which for more severe heating conditions transforms into a stable Fe_3B phase. On line monitoring of the electrical resistance variations allowed an accurate control of the heating procedure and of the resulting structural transformations, through the typical *R(I)* curves.

DSC analysis showed for the Fe-B-Zr-Cu a crystallization process that involves two clearly distinct phase transformations, for all the studied heating rates. Otherwise crystallization of Fe-B-Si-Ni-Mo samples followed different kinetics according to the applied heating rate: it exhibits multiple peaks for slow heating, and a single exothermal peak for heating rates equal or superior to 10 K/min. The obtained activation energies for the Fe-B-Zr-Cu alloy (362 and 301 kJ/mol) and for the Fe-B-Si-Ni-Mo alloy (323 kJ/mol) are comparable to reported values for amorphous iron alloys. The values of the Avrami exponents for Fe-B-Zr-Cu (n = 1.0 and 1.2) and for Fe-B-Si-Ni-Mo (n = 1.0) are consistent with diffusion controlled crystallization processes with nucleation rates close to zero.

Acknowledgments

This research was partially performed at LNLS - National Synchrotron Light Laboratory, Brazil. The authors thank financial support from CNPq (524262/96-9) and LNLS (0551-99).

References

1. Yoshizawa, Y.; Oguma, S.; Yamauchi, K. *J. Appl. Phys.*, v. 64, p. 6044, 1988.
2. Herzer, G. *IEEE Trans. Mag.*, v. 26, p. 1397, 1990.
3. Suzuki, K.; Makino, A.; Inoue, A.; Matsumoto, T. *Mater. Trans. JIM*, v. 32, p. 93, 1991.
4. Kim, B.G.; Song, J.S.'; Kim, H.S.; Oh, Y.W. *J. Appl. Phys.*, v. 77, p. 5298, 1995.
5. de Biasi, R.S.; Grillo, M.L.N. *J. Alloys Comp.*, v. 279, p. 233, 1998.
6. de Biasi, R.S.; dos Santos, D.S. *Mat. Sci. Forum*, v. 307, p. 107, 1999.
7. Vasquez, J.; Lopez-Alemany, P.L.; Villares, P.; Jiménez-Garay, R. *J. Alloys Comp.*, v. 61, p. 493, 2000.
8. dos Santos, D.S.; de Biasi, R.S. (submitted to *J. of Non- Crystalline Solids*).
9. Kopcewicz, M.; Grabias, A.; Williamson, D.L. *J. Appl. Phys.*, v. 82, p. 1747, 1997.
10. Lembke, U.; Hoell, A.; Kranold, R.; Müller, R.; Schüppel, W.; Goerigk, G.; Gilles, R.; Wiedenmann, A. *J. Appl. Phys.*, v. 85, n. 4, p. 2279, 1999.
11. dos Santos, D.R.; Torriani, I.; Silva, F.C.S.; Knobel, M. *J. Appl. Cryst.*, v. 33, p. 473, 2000.
12. dos Santos, D.R.; Torriani, I.; Silva, F.C.S.; Knobel, M. *J. Appl. Phys.*, v. 86, p. 6993, 1999.
13. Barandiarán, J.M.; Fernández Barquín, F.; Gómez Sal, J.C.; Gorria, P.; Hernando, A. *Sol. State Commun.*, v. 88, p. 75, 1993.
14. Allia, P.; Baricco, M.; Tiberto, P.; Vinai, F. *Phys. Rev. B*, v. 47, p. 3118, 1993.
15. Allia, P.; Baricco, M.; Knobel, M.; Tiberto, P.; Vinai, F. *Mater. Sci. Eng.*, v. A179-280, p. 361, 1994.
16. da Silva, F.C.S.; Ferrari, E.F.; Knobel, M.; Torriani, I.L.; dos Santos, D.R. *Appl. Phys. Letters*, v. 77, p. 1375, 2000.
17. Gao, Y.; Wang, W. *J. non-Cryst. Solids*, v. 81, p. 129, 1986.
18. Gao, Y.; Wang, W.; Zheng, F.Q.; Liu, X. *J. non-Cryst. Solids*, v. 81, p. 135, 1986.
19. Tolentino, H.; Cezar, J.C.; Cruz, D.Z.; Compagnon-Cailhol, V.; Tamura, E.; Martins Alves, M.C. *J. Synchr. Rad.*, v. 5, p. 521, 1998.
20. Torriani, I.; de Oliveira, C.; dos Santos, D.R.; Neuenschwander, R.; Kellerman, G.; Plivelic, T. *LNLS Newsletter*, v. 2, p. 4-5, 2000 (internal report, free download at www.lnls.br).
21. Ilschner, B. *Archiv f. d. Eisenhuttenwesen*, v. 26, p. 59, 1955.